TRANSIENT CHARACTERISTICS OF COUPLED THERMAL RADIATION AND NATURAL-CONVECTION IN A 3-D CYLINDRICAL CAVITY CONTAINING A HEATED PLATE

by

Tianxiang WANG[a], Yinan QIU[a], Gang LEI[a], Jinjin ZHANG[b], Yonghua HUANG[b], and Guang YANG[b]*

[a] State Key Laboratory of Technologies in Space Cryogenic Propellants, Beijing, China
[b] School of Mechanical Engineering, Shanghai Jiao Tong University, Shanghai, China

Original scientific paper
https://doi.org/10.2298/TSCI220523135W

In this study, a numerical study of transient combined natural-convection and surface radiation in a cylindrical cavity with a heated plate placed inside is carried out using the open-source platform OpenFOAM. The effects of the Rayleigh number ($10^5 \leq Ra \leq 10^7$), inclination angle ($0^o \leq \varphi \leq 90^o$), and surface emissivity ($0 \leq \varepsilon \leq 1$) on the velocity components, temperature field, and Nusselt number are investigated in detail. Results show that the Rayleigh number has a greater effect on the radiative heat transfer than on natural-convection. Radiative heat transfer increases monotonously with the increase of surface emissivity, and its contribution could be over 50% of the total heat transfer rate. The inclination angle of the plate affects the flow structure, but the difference in total Nusselt number is less than 10% for various inclination angles. Results in this study provide insights into the transient characteristics of coupled thermal radiation and natural-convection in a 3-D cavity and will guide the optimal design of related devices.

Key words: *natural-convection, radiation, numerical simulation, dynamic characteristics, heated plates*

Introduction

Understanding combined natural-convection and surface radiation in closed cavities has drawn tremendous interest due to its importance in substantial practical applications, including thermal cycling systems, nuclear reactors, chemical apparatus, data centre cooling, *etc.* Many of these applications can be simplified into physical models in which both natural-convection and surface radiation heat transfer happen in a closed cavity containing or not an internal heat source [1-12].

As both are directly determined by temperature differences, heat transfer induced by natural-convection and that by radiation are inherently strongly coupled. A vast amount of literature is available on such coupled heat transfer in 2-D enclosures under different boundary conditions. Notably, Sun *et al.* [10] conducted an experimental analysis to demonstrate the influence of radiation on the process of transition periodic flows in air-filled cavities. They found that surface radiation strengthened the re-circulation cells of flow along the vertical wall, which in turn stabilized flow fields for the specific configuration. Mezrhab *et al.* [8] numerically investigated the combined natural-convection and radiation in a differentially heated cavity

* Corresponding author, e-mail: y_g@sjtu.edu.cn

containing a centrally located square body. They showed that the radiation exchange achieved temperature homogenization inside the cavity and considerably increased the average Nusselt number. Moreover, the inner body induced an increase in the horizontal velocity when placed vertically in the centre in comparison with an empty cavity. Colomer *et al.* [6] numerically studied the coupling between radiation and convection in a differentially heated cavity using the discrete ordinates method. It was shown that surface radiation significantly increased the heat flux in a transparent medium for a given Planck number, while the contribution of radiation remained almost constant across a range of Rayleigh numbers. Transient combined natural-convection and radiation in a double space cavity with conducting walls was numerically studied by Nia *et al.* [13]. At a large value of the Rayleigh number, the temperature distribution in a thermal system was showed to be wavier in form. Yang and Wu [14] numerically studied the effects of natural-convection, wall thermal conduction, and thermal radiation on heat transfer from a heated plate located at the bottom of a rectangular enclosure. The increase of thermal radiation was found to restrain the convective heat transfer but increase the total heat transfer.

In engineering applications such as cooling problems, cylindrical hollow cavities are widely used, and they often have flow structures and thermal fields that are 3-D in space [5, 15-20]. Ghernoug *et al.* [15] numerically analyzed the effect of the Grashof number on natural-convection in an annular space between two eccentric horizontal cylinders. It was found that the thermal conduction was the dominant heat transfer regime for Grashof numbers lower than 5×10^4, while the convection governed the heat transfer and increased the value of the stream function for $5 \times 10^4 < \mathrm{Gr} < 1 \times 10^6$. Wu *et al.* [16] numerically investigated the effects of aperture position (angle) and size on the natural-convection heat loss of a solar heat-pipe receiver. It was found that increased aperture might bring about impressive increment of natural-convection heat loss at intermediate angles, while natural-convection heat loss appeared to be an insignificant increment at sideward and downward orientations. Zhang *et al.* [17] numerically studied natural-convection in two and 3-D simulations of cylinders with slots. They pointed out that the 3-D numerical simulations could reflect the oscillation phenomenon in the cavity, but the same could not be simulated by 2-D numerical methods. Wu *et al.* [18] numerically investigated the combined heat loss characteristic of a hollow cylinder with one vertical side open and the inner walls of its cavity heated by constant heat flux. It was found that the natural convective Nusselt number, Nu_c, decreased, and the radiative Nusselt number, Nu_r, increased when the tilt angle was changed from 0°-90°. Also, the coupled heat transfer by natural-convection and radiation in an upward-facing cylindrical cavity with different tilt angles, heat fluxes and surface heating conditions was investigated experimentally and numerically by Shen *et al.* [19], and the extremum of heat transfer among varying tilt angles was observed to be at the angle between –45° and –30°. In a less similar study, the flow and heat transfer of electrohydrodynamic natural-convection in the annulus between a rectangular and a circular cylinder was numerically investigated by Roy *et al.* [20]. The locally distributed Nusselt number at the inner and outer cylinders confirmed that thermal radiation was the dominant mode of heat transfer. An investigation of the coupled heat transfer in a vertical hollow cylinder with finite wall thickness was carried out by Chandrakar *et al.* [5], where correlations for Nusselt number were proposed that considered both natural-convection and surface radiation.

Despite the aforementioned, the coupling between thermal radiation and natural-convection heat transfer in a 3-D cylindrical cavity is still far from fully understood, especially for the transient heat transfer situations with an internal heat source. Moreover, previous studies indicated that the heat transfer characteristics in such a 3-D domain could not be fully reflected by a 2-D numerical method. Therefore, this study aims to numerically investigate the coupled heat transfer process in a cylindrical cavity with a heated plate located inside, considering large ranges of Rayleigh numbers, emissivity of surfaces and inclination angles of the heated plate. Another important purpose of the present study is to understand the transient characteristics of the coupled heat transfer, which was less considered by previous studies yet essential in many practical applications.

Mathematical formulation

The schematic diagram of the physical model in this study is a 3-D cylindrical cavity with length, L, and diameter, D, containing a heated rectangle plate ($L\times W\times H$) placed in the cavity at different inclined angles, as shown in fig. 1. The solid plate is maintained at uniform hot temperature T_h, and the cylindrical surface is isothermally cooled at a temperature T_c, while the circular ends are adiabatic (the net heat fluxes by natural-convection and radiation are zero). The surfaces of cavity and plate are assumed to be opaque, gray, and diffuse emitters and reflectors of radiation with an emissivity, ε. The gravity acts downward normal to the XZ plane. The tilt angle, φ, of the plate varies from the horizon the vertical with respect to the direction of gravity. The working fluid is air, a non-emitting, non-absorbing, and non-participating medium. All the thermo-physical properties are assumed to be constant, except for the buoyancy term in the momentum equation for which the Boussinesq approximation has been adopted [21, 22]. The flow in the cavity is assumed to be laminar and incompressible. No-slip velocity conditions are assumed at the solid walls.

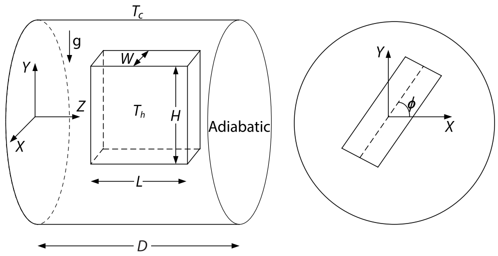

Figure 1. Schematics for the problem of conjugate natural-convection combined with surface thermal radiation in a cylindrical cavity with a heated plate inside at an angle

The governing equations of the fluid zone can be written:

$$\frac{\partial u}{\partial x}+\frac{\partial v}{\partial y}+\frac{\partial w}{\partial z}=0 \tag{1}$$

$$\frac{\partial u}{\partial t}+u\frac{\partial u}{\partial x}+v\frac{\partial u}{\partial y}+w\frac{\partial u}{\partial z}=-\frac{1}{\rho}\frac{\partial p}{\partial x}+\nu\left(\frac{\partial^2 u}{\partial x^2}+\frac{\partial^2 u}{\partial y^2}+\frac{\partial^2 u}{\partial z^2}\right) \tag{2}$$

$$\frac{\partial v}{\partial t}+u\frac{\partial v}{\partial x}+v\frac{\partial v}{\partial y}+w\frac{\partial v}{\partial z}=-\frac{1}{\rho}\frac{\partial p}{\partial y}+\nu\left(\frac{\partial^2 v}{\partial x^2}+\frac{\partial^2 v}{\partial y^2}+\frac{\partial^2 v}{\partial z^2}\right)+\mathrm{g}\beta\left(T-T_\mathrm{c}\right) \tag{3}$$

$$\frac{\partial w}{\partial t}+u\frac{\partial w}{\partial x}+v\frac{\partial w}{\partial y}+w\frac{\partial w}{\partial z}=-\frac{1}{\rho}\frac{\partial p}{\partial z}+\nu\left(\frac{\partial^2 w}{\partial x^2}+\frac{\partial^2 w}{\partial y^2}+\frac{\partial^2 w}{\partial z^2}\right) \tag{4}$$

$$\frac{\partial T}{\partial t}+u\frac{\partial T}{\partial x}+v\frac{\partial T}{\partial y}+w\frac{\partial T}{\partial z}=\alpha\left(\frac{\partial^2 T}{\partial x^2}+\frac{\partial^2 T}{\partial y^2}+\frac{\partial^2 T}{\partial z^2}\right) \tag{5}$$

The initial condition and the boundary conditions are:

$$\begin{aligned}&t=0: u=v=w=0, T=T_\mathrm{c}, \text{ at } x^2+y^2\le D^2,\ 0\le z\le D\\ &t>0: u=v=w=0,\ T=T_\mathrm{c}, \text{ at } x^2+y^2=D^2,\ 0<z<D\end{aligned} \tag{6}$$

$\rightarrow$

$$u = v = w = 0,\ \frac{\partial T}{\partial z} = \frac{q_{\mathrm{rd}}}{\kappa},\ \text{at}\ \ x^2 + y^2 \le D^2,\ z = 0$$

$$u = v = w = 0,\ \frac{\partial T}{\partial z} = \frac{-q_{\mathrm{rd}}}{\kappa},\ \text{at}\ x^2 + y^2 \le D^2,\ z = D$$

$$u = v = w = 0\ \text{and}\ T = T_{\mathrm{h}}\ \textit{at}\ \text{the plate surfaces}$$

The total radiative flux is determined by the difference between the incident energy q_i and the radiosity q_o using the net-radiation method [23]. The solid surfaces are divided into N discrete surface elements. Thus, the radiation heat balance for the k^{th} surface element provides the relation:

$$q_{\mathrm{rad},k} = q_{o,k} - q_{i,k},\ k = 1...N \tag{7}$$

$$q_{o,k} = \varepsilon_k \sigma T_k^{\ 4} + \left(1 - \varepsilon_k\right) q_{i,k},\ k = 1...N \tag{8}$$

$$q_{i,k} = \sum_{j=1}^{N} F_{kj} q_{o,j},\ k = 1...N \tag{9}$$

where the quantities $q_{o,k}$ and $q_{i,k}$ are the incoming and outgoing radiant energy rates for the k^{th} differential element. The interaction between radiative and convective energy flow brings about the net fluxes on the k^{th} differential element.

In order to investigate the coupling mechanism between natural-convection and surface radiation, the following dimensionless variables are introduced:

$$\begin{gathered}
X = \frac{x}{D},\ Y = \frac{y}{D},\ Z = \frac{z}{D},\ \theta = \frac{T - T_{\mathrm{c}}}{\Delta T},\ P = \frac{p}{D\rho \mathrm{g}\beta\Delta T} \\
U = \frac{u}{\sqrt{D\mathrm{g}\beta\Delta T}},\ V = \frac{v}{\sqrt{D\mathrm{g}\beta\Delta T}},\ W = \frac{w}{\sqrt{D\mathrm{g}\beta\Delta T}},\ \tau = t\sqrt{\frac{\mathrm{g}\beta\Delta T}{D}} \\
\mathrm{Pr} = \frac{\nu}{\alpha},\ \mathrm{Ra} = \frac{\mathrm{g}\beta\Delta T D^3}{\nu\alpha},\ N_{RC} = \frac{\sigma T_{\mathrm{h}}^{\ 4} D}{\kappa\Delta T},\ Q_{\mathrm{rd}} = \frac{q_{\mathrm{rd}}}{\sigma T_{\mathrm{h}}^{\ 4}} \\
R_k = \frac{q_{o,k}}{\sigma T_{\mathrm{h}}^4},\ I_k = \frac{q_{i,k}}{\sigma T_{\mathrm{h}}^4},\ \Theta_k = \frac{T_k}{T_{\mathrm{h}}},\ Q_{\mathrm{rd},k} = \frac{q_{\mathrm{rd},k}}{\sigma T_{\mathrm{h}}^4}
\end{gathered} \tag{10}$$

The governing equations eqs. (1)-(5) could therefore, be written in the dimensionless form as:

$$\frac{\partial U}{\partial X} + \frac{\partial V}{\partial Y} + \frac{\partial W}{\partial Z} = 0 \tag{11}$$

$$\frac{\partial U}{\partial \tau} + U\frac{\partial U}{\partial X} + V\frac{\partial U}{\partial Y} + W\frac{\partial U}{\partial Z} = -\frac{\partial P}{\partial X} + \sqrt{\frac{\mathrm{Pr}}{\mathrm{Ra}}}\left(\frac{\partial^2 U}{\partial X^2} + \frac{\partial^2 U}{\partial Y^2} + \frac{\partial^2 U}{\partial Z^2}\right) \tag{12}$$

$$\frac{\partial V}{\partial \tau} + U\frac{\partial V}{\partial X} + V\frac{\partial V}{\partial Y} + W\frac{\partial V}{\partial Z} = -\frac{\partial P}{\partial Y} + \sqrt{\frac{\mathrm{Pr}}{\mathrm{Ra}}}\left(\frac{\partial^2 V}{\partial X^2} + \frac{\partial^2 V}{\partial Y^2} + \frac{\partial^2 V}{\partial Z^2}\right) + \theta \tag{13}$$

$$\frac{\partial W}{\partial \tau}+U\frac{\partial W}{\partial X}+V\frac{\partial W}{\partial Y}+W\frac{\partial W}{\partial Z}=-\frac{\partial P}{\partial Z}+\sqrt{\frac{\mathrm{Pr}}{\mathrm{Ra}}}\left(\frac{\partial^2 W}{\partial X^2}+\frac{\partial^2 W}{\partial Y^2}+\frac{\partial^2 W}{\partial Z^2}\right) \tag{14}$$

$$\frac{\partial \theta}{\partial \tau}+U\frac{\partial \theta}{\partial X}+V\frac{\partial \theta}{\partial Y}+W\frac{\partial \theta}{\partial Z}=\frac{1}{\sqrt{\mathrm{RaPr}}}\left(\frac{\partial^2 \theta}{\partial X^2}+\frac{\partial^2 \theta}{\partial Y^2}+\frac{\partial^2 \theta}{\partial Z^2}\right) \tag{15}$$

With the previous dimensionless forms correspond, respectively to the boundary conditions:

$$\begin{gathered}\tau=0: U=V=W=0,\ \theta=0,\ \text{at}\ X^2+Y^2=1,\ 0\le Z\le 1\\ \tau>0: U=V=W=0,\ \theta=0,\ \text{at}\ X^2+Y^2=1,\ 0<Z<1\\ U=V=W=0,\ \frac{\partial \theta}{\partial Z}=N_{RC}Q_{\mathrm{rd}},\ \text{at}\ X^2+Y^2\le 1,\ Z=0\\ U=V=W=0,\ \frac{\partial \theta}{\partial Z}=-N_{RC}Q_{\mathrm{rd}},\ \text{at}\ X^2+Y^2\le 1,\ Z=1\\ U=V=W=0,\ \theta=1\ \text{at the plate surfaces}\end{gathered} \tag{16}$$

For the net radiative heat flux equations, eqs. (7)-(9) of the k^{th} solid-fluid differential element, the dimensionless form is obtained:

$$Q_{\mathrm{rd},k}=R_k-I_k,\ k=1...N \tag{17}$$

$$R_k=\varepsilon_k\theta_k^4+\left(1-\varepsilon_k\right)I_k,\ k=1...N \tag{18}$$

$$I_k=\sum_{j=1}^{N}F_{kj}R_j,\ k=1\ldots N \tag{19}$$

In order to investigate the effect of different variables on the heat transfer, the local convective and radiative heat transfer rates on the cylindrical face were evaluated by the average Nusselt number. The total average Nusselt number on the cylindrical face was taken as the sum of the average convective and radiative Nusselt numbers:

$$\mathrm{Nu}_{\mathrm{cv}}=\frac{h_{\mathrm{cv}}D}{\lambda_a}=\frac{q_{\mathrm{cv}}}{\lambda_a\Delta T\pi D} \tag{20}$$

$$\mathrm{Nu}_{\mathrm{rd}}=\frac{h_{\mathrm{rd}}D}{\lambda_a}=\frac{q_{\mathrm{rd}}}{\lambda_a\Delta T\pi D} \tag{21}$$

$$\mathrm{Nu}=\mathrm{Nu}_{\mathrm{cv}}+\mathrm{Nu}_{\mathrm{rd}} \tag{22}$$

Numerical procedure

The governing equations were discretized using the finite volume method on collocated, structured and partial non-uniform grids system. The third-order QUICK scheme and the second-order central difference scheme were used for the convection and diffusion terms, respectively. The PIMPLE algorithm was used for the coupling velocity-pressure terms in the transient process, which was a combination of semi-implicit method for pressure-linked equations (SIMPLE) algorithm and pressure implicit with splitting of operator (PISO) algorithm [24]. The view factors were solved by the cross-string method [23]. The time step was further set to ensure the flow courant number remained under 0.3. The solution was considered to converge when the relative variation of any variable was below 10^{-6}.

The simulations in this study were conducted using the open source platform OpenFOAM (v5.0) [24]. The accuracy of the present numerical approach in solving the coupled heat transfer problem is validated, with the case of the coupled radiation and natural-convection in an air-filled square cavity. For a 2-D cavity with an internal plate, it is observed from fig. 2 that the results were consistent with those of Saravanan and Sivaraj [25]. The maximum deviation in the average Nusselt number was approximately 4%. Therefore, the numerical method proves to be accurate enough for simulating coupled heat transfer in cavities with a heat source located inside. The grid independence test was carried out to examine the dependence of numerical accuracy on grid density. Table 1 shows the variation of average Nusselt numbers with an increase of the number of grids. The difference was below 0.2% when the grid number reached 10.2×10^5. Hence, the grid number 10.2×10^5 was adopted for the simulations.

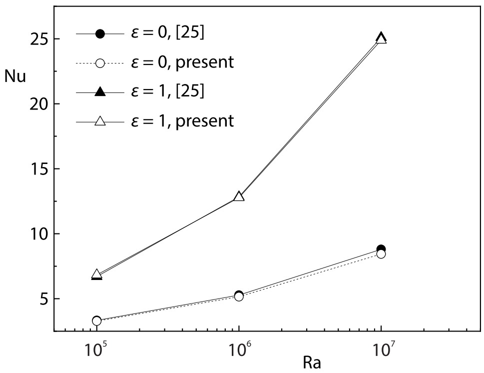

Figure 2. Comparison of Nusselt number with [25] (plate length: *h/L* = 0.5)

Table 1. Effect of grid number on the average Nusselt number on the cylindrical surface for the case of Ra = 10^6, *W/D* = 1/8, *L/D* = 1/2, *H/D* = 1/2, ε = 1, φ = 90º

Grid number	4.2×10^5	7.2×10^5	10.2×10^5	13.4×10^5	16.4×10^5
$\overline{\text{Nu}}$	8.34769	8.34124	8.33878	8.33792	8.33090

Results and discussion

A numerical study of the combined surface radiation and natural-convection heat transfer in a hollow cylinder with a heat plate located inside was carried out. The effects of dimensionless time, τ, surface emissivity, ε, Rayleigh number, and inclination angle of the internal plate, φ, on fluid-flow and heat transfer were investigated. The values of the parameters were given as $10^5 \leq \text{Ra} \leq 10^7$, $0º \leq \varphi \leq 90º$, $0 \leq \varepsilon \leq 1$, $W/D = 1/8$, $L/D = 1/2$, $H/D = 1/2$, and Pr = 0.71, which corresponds to a typical cooling problem [5, 11-12, 15]. The reference temperature of air was set as $T_0 = (T_c + T_h)/2 = 303.15$ K, and the temperature difference between the cold cylindrical wall and the hot plate surface was kept at a constant value of 20 K, for which the Boussinesq approximation was valid. The reference pressure of air was 100 kPa, and the thermal expansion coefficient was set as 0.0033 1/K. All the computations were conducted in the transient process until reaching steady-state.

Flow pattern and temperature field

Figure 3 shows the isotherms for the middle of the planes *XY* (Z = 0.5) and *XZ* (Y = 0) at Ra = 10^6, φ = 0º, ε = 1 for different dimensionless times. The isotherms tended to move closer to the centre axis at the location above the plate, where two symmetrical thermal plumes form and develop for $\tau < 10$, figs. 3(a)-3(c). This process highlights that natural-convection first occurs near the upper corners of the heated plate as the fluid gets heated and starts to rise, driven by buoyancy. Further increase in the dimensionless time ($\tau > 10$) led to the merging of the thermal plumes above the plate, figs. 3(g)-3(i). Also, the isotherms in the *XZ* plane, figs. 3(d)-3(f), and 3(j)-3(l) tended to become non-uniform as the transport process developed.

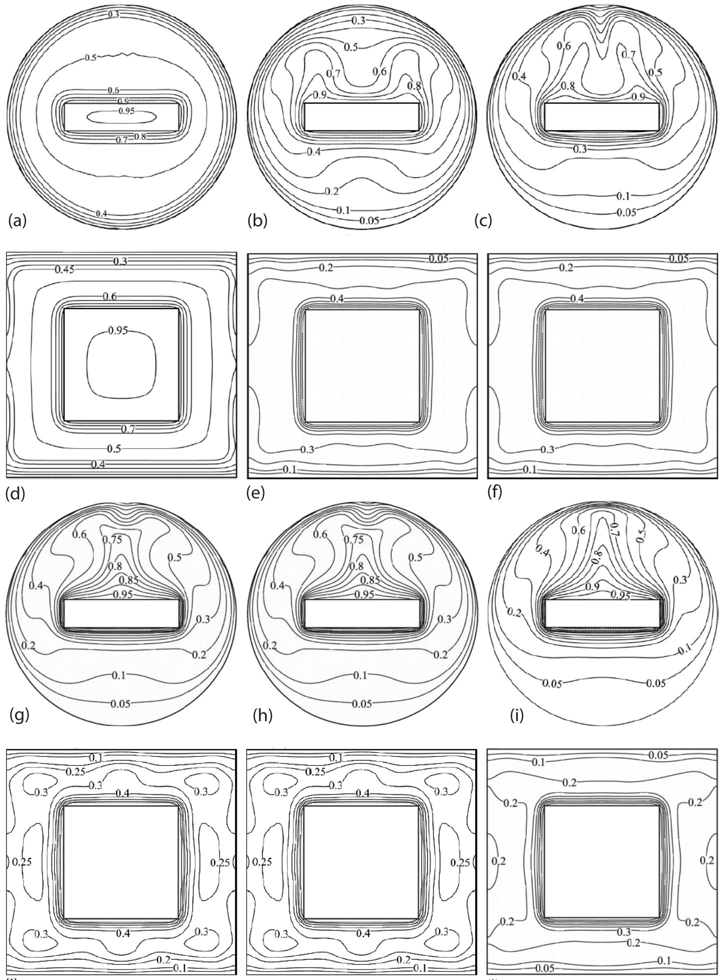

Figure 3. Dynamic evolution of isotherms Θ on the *XY* plane (Z = 0.5) and the *XZ* plane (Y = 0) for Ra = 10^6, φ = 0º, ε = 1, (a) τ = 1, Z = 0.5, (b) τ = 5, Z = 0.5, (c) τ = 10, Z = 0.5, (d) τ = 1, Y = 0, (e) τ = 5, Y = 0, (f) τ = 10, Y = 0, (g) τ = 13, Z = 0.5, (h) τ = 14, Z = 0.5, (i) τ = 100, Z = 0.5, (j) τ = 13, Y = 0, (k) τ = 14, Y = 0, and (l) τ = 100, Y = 0

Figure 4(a) shows the evolution of the temperature profiles along the y-direction on the centerline of the *XY* plane (Z = 0.5) with time for the case of Ra = 10^6, φ = 0º, ε = 1. Following an initial oscillating stage at τ < 10, the temperature above the plate increased and that below the plate decreased with time, with both tending to steady-states. The development of the temperature profile significantly affected the velocity, as shown in fig. 4(b), which illustrates the velocity component V_y along the y-direction at the same location fig. 4(a) describes. The maximum value of the velocity increased for τ > 10, especially for locations above the heated plate. Steady-state was found to be achieved before τ = 100 by fact of the invariability of the velocity in fig. 4(b) and of temperature in fig. 4(a) for τ > 100.

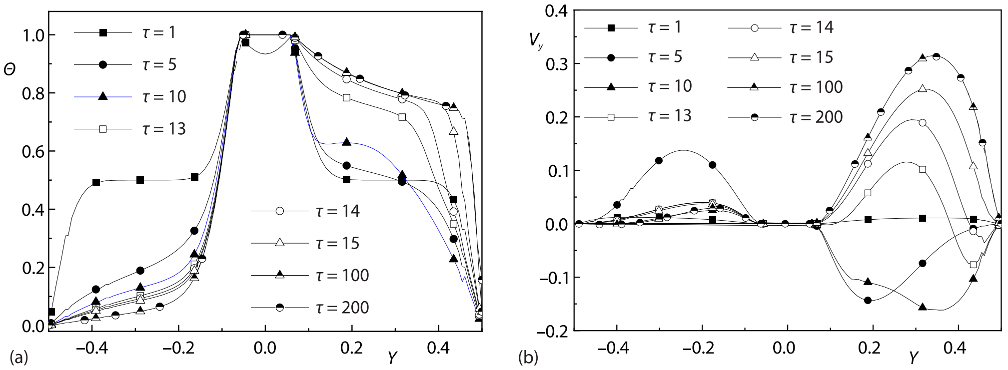

Figure 4. Distributions of (a) temperature and (b) velocity component V_y along y-direction (X = 0, Z = 0.5) for Ra = 10^6, φ = 0º, ε = 1 and different evolution time

Effect of the surface emissivity

The steady-state isotherms in the middle of the XY (Z = 0.5) and XZ (Y = 0) planes for different emissivity values with Ra = 10^6, φ = 90º are displayed in fig. 5. The isotherms in the horizontal direction, figs. 5(d)-(f) were found to be more significantly affected by surface emissivity than those in the vertical direction, figs. 5(a)-5(c), and the shape of the isotherms became complex as the value of surface emissivity increased. In general, the fluid temperature increased with increased surface emissivity, *e.g.*:

$$\Theta_{y=-0.4}^{\varepsilon=0} = 0.027,\ \Theta_{y=-0.4}^{\varepsilon=0.2} = 0.02,\ \Theta_{y=-0.4}^{\varepsilon=0.5} = 0.031,\ \Theta_{y=-0.4}^{\varepsilon=0.8} = 0.0315,\ \Theta_{y=-0.4}^{\varepsilon=1} = 0.032$$

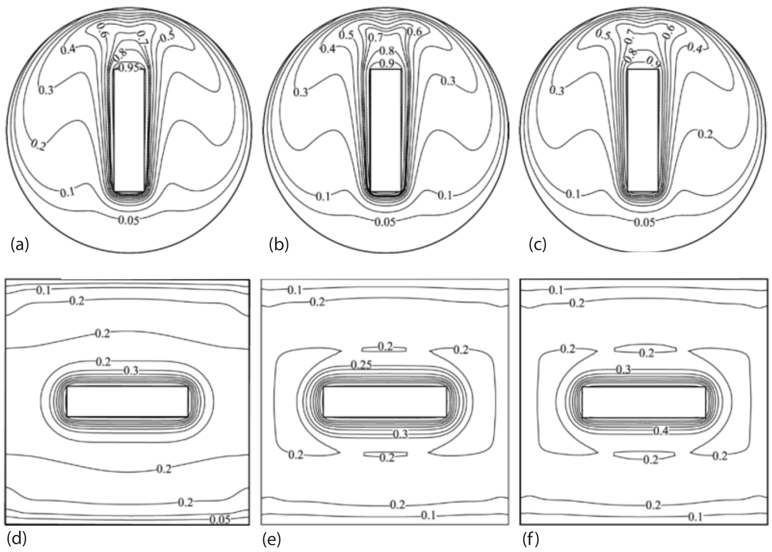

Figure 5. Steady-state isotherms Θ on the XZ plane (Y = 0) and the XY plane (Z = 0.5) for different surface emissivity values at Ra = 10^6, φ = 90º, τ = 100; (a) ε = 0, Z = 0.5, (b) ε = 0.5, Z = 0.5, (c) ε = 1, Z = 0.5, (d) ε = 0, Y = 0, (e) ε = 0.5, Y = 0, and (f) ε = 1, Y = 0

The reason for this phenomenon is the coupled effect of the radiation and natural-convection, as the side walls were heated due to surface radiation from the heater, which, thereafter, heated the fluid in the boundary-layer via natural-convection. This explanation is supported by the distributions of temperature, as temperatures were found to be most increased in the vicinity of the sidewalls of the cylinder by the increase of surface emissivity, as shown in fig. 6.

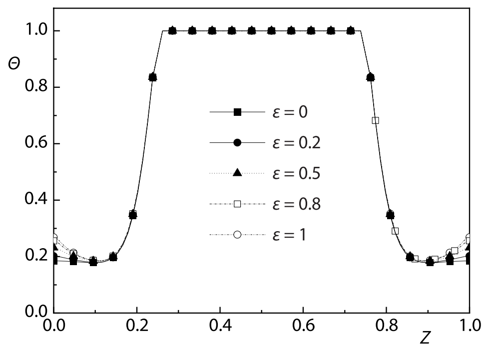

Figure 6. Distributions of temperature along *Z* direction ($Y = X = 0$) for Ra = 10^6, $\varphi = 90^\circ$, $\tau = 100$ and different surface emissivity values

The steady-state profiles of the velocity component along *Z* direction is presented in fig. 7 for Ra = 10^6, φ = 90º and different values of surface emissivity. It was demonstrated that the velocity component in the vertical direction, V_y, is two order of magnitude larger than other directions, which is due to the buoyancy effect. As inferred from the figures, the intensity of natural-convection (determined from the velocity near the walls) in the cavity increases with the increase of surface emissivity.

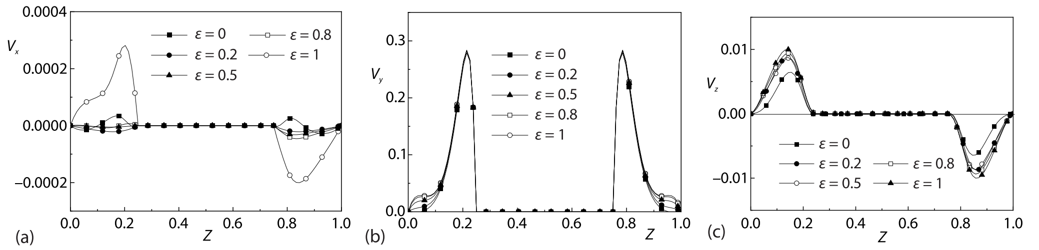

Figure 7. Distribution of the steady-state velocity component along *Z* direction for Ra = 10^6, $\varphi = 90^\circ$ and different surface emissivity values; (a) V_x, $Y = X = 0$, (b) V_y, $Y = X = 0$, and (c) V_z, $Y = X = 0$

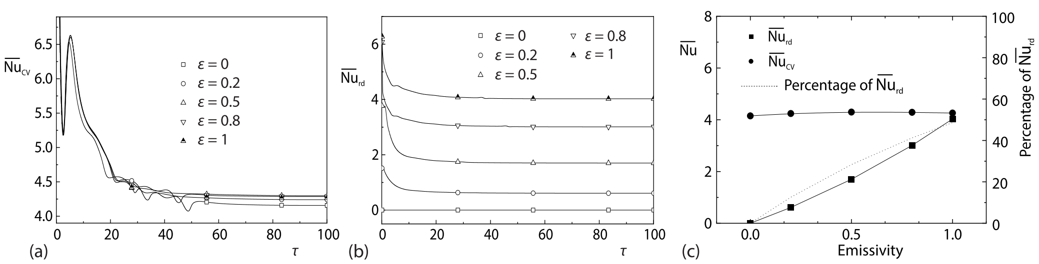

Figure 8. Variation of the average (a) convective and (b) radiative Nusselt number on the cylindrical face with time, and (c) the steady-state total Nusselt number for Ra = 10^6, $\varphi = 90^\circ$, and different surface emissivity values

The effect of the surface emissivity on the average Nusselt numbers of the cylindrical face is presented in fig. 8. The radiative heat transfer increased almost linearly with the increase of surface emissivity, *e.g.*:

$$\mathrm{Nu}_{\mathrm{rd}}^{\varepsilon=0} = 0,\ \mathrm{Nu}_{\mathrm{rd}}^{\varepsilon=0.2} = 0.6,\ \mathrm{Nu}_{\mathrm{rd}}^{\varepsilon=0.5} = 1.7,\ \mathrm{Nu}_{\mathrm{rd}}^{\varepsilon=0.8} = 3.0,\ \mathrm{Nu}_{\mathrm{rd}}^{\varepsilon=1} = 4.0$$

at steady-state, while the convective Nusselt number remained almost unchanged, as its value varied between 4.1 and 4.3 for $0 \leq \varepsilon \leq 1$. Consequently, for the total Nusselt number, the contribution by the average radiative Nusselt number increased from 0-48.6% as the surface emissivity increased from 0-1 for Ra = 10^6.

Effect of the Rayleigh number

Figure 9 shows the steady-state isotherms on the middle planes of XY (Z = 0.5) and XZ (Y = 0) for ε = 1, φ = 90º and different Rayleigh numbers. The temperature gradient was found to increase around the plate and at the upper zones of a cylinder with increase in the Rayleigh number, indicating a higher heat flux. As the Rayleigh number increased, a downward flow (negative V_y) occurred above the heated plate, as shown in fig. 10(a). When the Rayleigh number increased to 10^7, two additional velocity peaks appeared near the adiabatic walls, figs. 10(b)-10(c), indicating a more complex flow field.

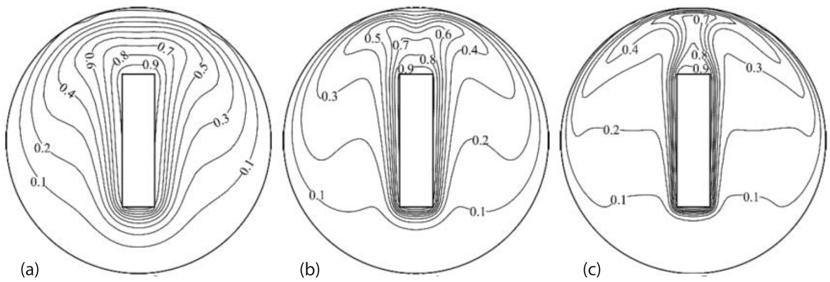

Figure 9. Steady-state isotherms Θ on the XY plane (Z = 0.5) for ε = 1, φ = 90º and different Rayleigh numbers; (a) Ra = 10^5, Z = 0.5, (b), Ra = 10^6, Z = 0.5, and (c) Ra = 10^7, Z = 0.5

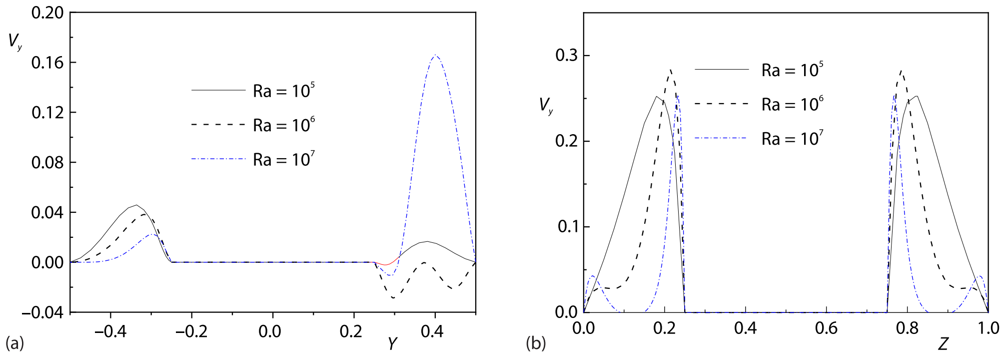

Figure 10. Distribution of the steady-state velocity component along the y-direction at the centerlines of the XY plane (Z = 0.5) and the XZ cross-section (Y = 0) for ε = 1, φ = 90º, τ = 100 and different Rayleigh numbers; (a) Z = 0.5, X = 0 and (b) Y = X = 0

Figure 11 plots the variation of the average Nusselt numbers on the cylindrical face *vs.* the Rayleigh numbers for ε = 1 and φ = 90º. From fig. 11(a), it can be seen that a longer time is needed to reach steady-state for a higher Rayleigh number. Both the radiative Nusselt number and the convective Nusselt number increased with increase of the Rayleigh number. However, the contributon of radiative Nusselt number increased from 42.8-53.1% as the Rayleigh number increased from 10^5 to 10^7 for ε = 1, indicating that the Rayleigh number has a stronger effect on radiative heat transfer than on convective heat transfer, fig. 11(b). This finding is also in agreement with that in [14].

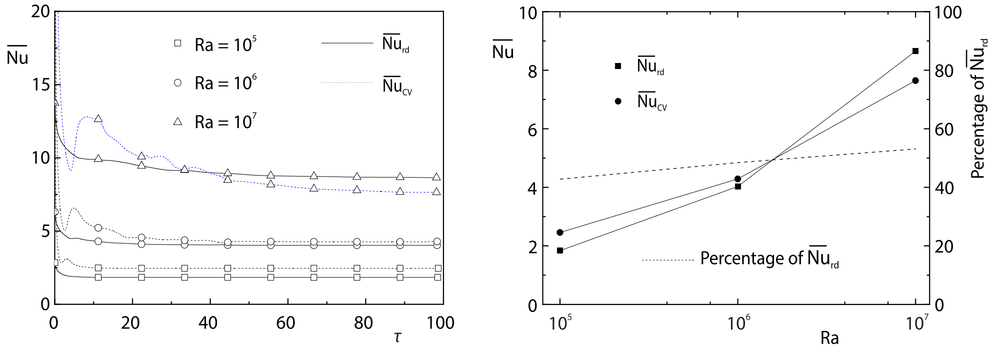

Figure 11. Variation of (a) the average Nusselt number on the cylindrical face with time and (b) the steady-state Nusselt number for ε = 1, φ = 90° and different Rayleigh numbers

Effect of the inclination angle of the plate

The effect of the inclination angle of the plate on the isotherms is illustrated in fig. 12. As the plate's inclination angle varied, the shape of the thermal plumes above the plate shifted accordingly. Figure 13(a) depicts the more detailed variation of the dimensionless temperature along the y-direction depending on the inclination angle. The variation trend of the steady-state temperature shows to be non-monotonic, and the minimum value above the heated plate was found to be at φ = 45°. This phenomenon could be explained by the larger values of V_x in the non-symmetry geometries as shown in fig. 13(b).

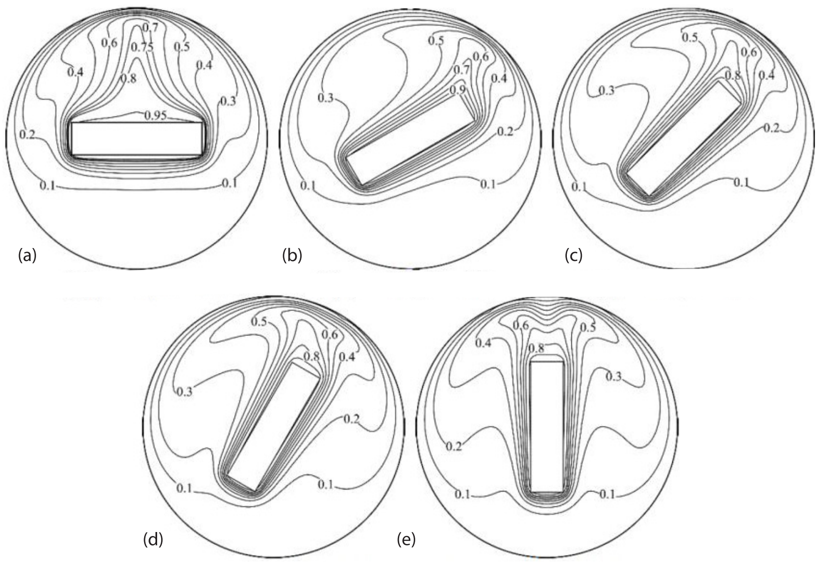

Figure 12. Steady-state isotherms Θ for the XY plane (Z = 0.5) with Ra = 10⁶, ε = 0.5 at different inclination angles; (a) φ = 0°, Z = 0.5, (b), φ = 30°, Z = 0.5, (c), φ = 45°, Z = 0.5, (d) φ = 60°, Z = 0.5, and (e) φ = 90°, Z = 0.5,

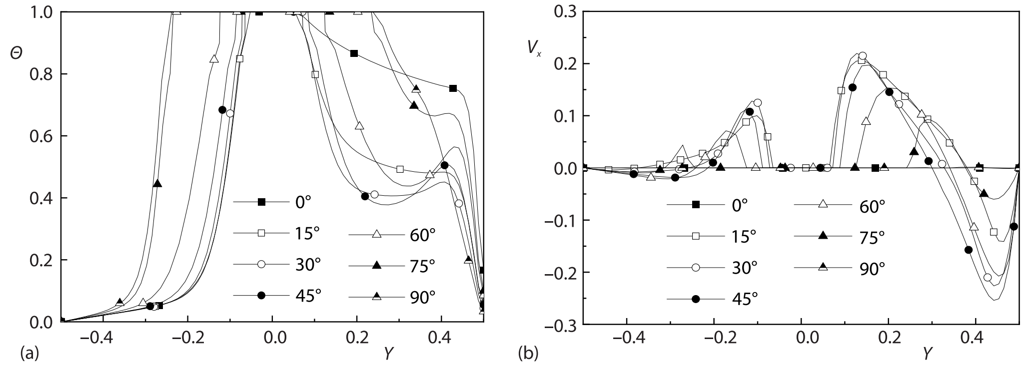

Figure 13. Profiles of the (a) temperature and (b) velocity components V_x along the *y*-direction at the centerline of the *XY* cross-section (Z = 0.5) with Ra = 10^6, ε = 0.5, τ = 100 at different inclination angles

Figure 14 presents the variation of the average Nusselt number at the cylindrical face with dimensionless time at different inclination angles for Ra = 106, ε = 0.5. A similar oscillation of average Nusselt numbers was found at the initial time for all angles, which then tended to stabilize differently for different inclination angles. The convective Nusselt number increased gradually as the inclination angle changed from φ = 0º to φ = 90º, *e.g.*,

$$\overline{\mathrm{Nu}}_{\mathrm{cv}}^{\varphi=0^\circ} = 3.92,\ \overline{\mathrm{Nu}}_{\mathrm{cv}}^{\varphi=15^\circ} = 4.00,\ \overline{\mathrm{Nu}}_{\mathrm{cv}}^{\varphi=30^\circ} = 4.12,\ \overline{\mathrm{Nu}}_{\mathrm{cv}}^{\varphi=45^\circ} = 4.20,\ \overline{\mathrm{Nu}}_{\mathrm{cv}}^{\varphi=60^\circ} = 4.28$$

$$\overline{\mathrm{Nu}}_{\mathrm{cv}}^{\varphi=75^\circ} = 4.31,\ \overline{\mathrm{Nu}}_{\mathrm{cv}}^{\varphi=90^\circ} = 4.29$$

As the inclination angle increased, an *M* shape distribution of radiative heat transfer was evident, with the local minimum values occurring at φ = 0º, 45º and 90º. Non-etheless, the change in the total Nusselt number, resulting from the variation of inclination angle, was less than 10%.

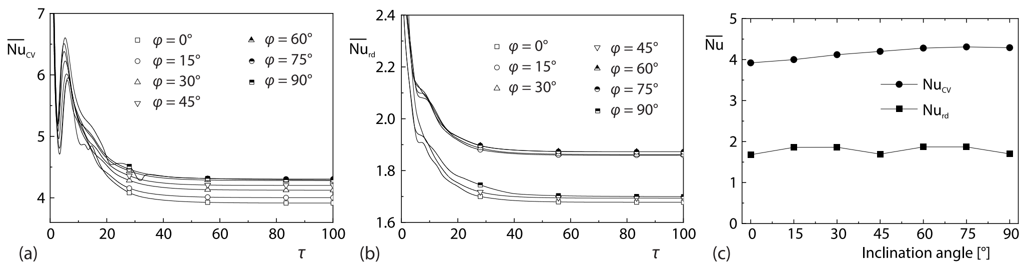

Figure 14. Variation of the average (a) convective and (b) radiative Nusselt number on the cylindrical face with time and (c) variation of steady-state Nusselt number with inclination angle

Conclusions

The transient heat transfer characteristics of coupled thermal radiation and natural-convection in a 3-D cylindrical cavity with a heated plate inside were numerically studied, and the isotherms, velocity component profiles, and Nusselt numbers investigated for a large range of governing parameters, including surface emissivity $0 \leq \varepsilon \leq 1$, Rayleigh number $10^5 \leq \mathrm{Ra} \leq 10^7$ and inclination angle $0º \leq \varphi \leq 90º$.

Due to the buoyancy effect, two thermal plumes form at the corners of the heated plate and finally merge above the heated plate. The velocity component in the vertical direction, V_y, is one order of magnitude larger than the component in other directions for symmetrical geometries. The radiative heat transfer increases linearly with increase of surface emissivity, but the variation in convective Nusselt number is insignificant.

As Rayleigh number increases, the intensity of natural-convection increases. Both the radiative Nusselt number and the convective Nusselt number increase with increasing Rayleigh number. However, the ratio of the radiative Nusselt number to the Rayleigh number increases as the Rayleigh number increases from 10^5 to 10^7, indicating that the Rayleigh number has a stronger effect on radiative heat transfer than convective heat transfer.

As the inclination angle increases from 0º-90º, the convective Nusselt number increases monotonously, while the radiative heat transfer decreases and then increases. However, the difference in the total Nusselt number for various inclination angles is less than 10%.

Acknowledgment

This work is supported by the National Natural Science Foundation of China (51936006), and the fund of the State Key Laboratory of Technologies in Space Cryogenic Propellants (SKLTSCP202005).

Nomenclature

D – length and diameter of the cylinder, [m]
F_{kj} – view factor from k^{th} element to j^{th} element, [–]
g – gravitational acceleration, [ms^{-2}]
H – height of the plate, [m]
h – heat transfer coefficient, [Wm^{-2}K^{-1}]
I_k – dimensionless irradiation of the k^{th} element, [–]
k – thermal conductivity, [Wm^{-1}K^{-1}]
L – length of the plate, [m]
N – total number of radiative elements, [–]
Nu – Nusselt number (=hD/k), [–]
P – dimensionless pressure, [–]
p – pressure, [Pa]
Pr – Prandtl number (=ν/a), [–]
Q_{rd} – dimensionless net radiative flux, [–]
q – thermal flux, [Wm^{-2}]
Ra – Rayleigh number (=$g\beta\Delta TD^3)/\nu a$), [–]
R_k – dimensionless radiosity of the k^{th} element, [–]
T – temperature, [K]
t – time, [s]
U, V, W – dimensionless velocity components, [–]
u, v, w – velocity components, [ms^{-1}]
W – width of the plate, [m]
X, Y, Z – dimensionless co-ordinates, [–]
x, y, z – Cartesian co-ordinates, [m]

Greek symbols

α – thermal diffusivity of fluid, [m^{2}s^{-1}]
β – coefficient of thermal expansion, [K^{-1}]
ε – emissivity of the radiative surface, [–]
θ – dimensionless temperature, [–]
ν – kinematic viscosity, [m^{2}s^{-1}]
ρ – air density, [kgm^{-3}]
σ – Stefan-Boltzmann constant, [Wm^{-2}K^{-4}]
τ – dimensionless time, [–]
φ – inclination angle, [º]

Subscripts

c – cold surfaces
h – hot surfaces
cv – convection
r – radiative
rd – radiation

References

[1] Cheng, T. C., *et al.*, Combined Natural-Convection and Radiation with Temperature-Dependent Properties, *Thermal Science, 22* (2018), 2, pp. 921-930
[2] Astanina, M. S., *et al.*, Effect of Thermal Radiation on Natural-Convection in a Square Porous Cavity Filled with a Fluid of Temperature-Dependent Viscosity, *Thermal Science, 22* (2018), 1B, pp. 391-399
[3] Qasem, S. A., *et al.*, Effect of Thermal Radiation on Natural Conviction of a Nanofluid in a Square Cavity with a Solid Body, *Thermal Science, 25* (2021), 3A, pp. 182-182
[4] Benyahia, N., *et al.*, Coupling Turbulent Natural-Convection-Radiation-Conduction in Differentially Heated Cavity with High Aspect Ratio, *International Journal of Thermal Sciences, 158* (2020), 106518

[5] Chandrakar, V., *et al.*, Conjugate Heat Transfer Due to Conduction, Natural-Convection, and Radiation from a Vertical Hollow Cylinder with Finite Thickness, *Numerical Heat Transfer, Part A, 79* (2021), 6, pp. 463-487
[6] Colomer, G., *et al.*, 3-D Numerical Simulation of Convection and Radiation in a Differentially Heated Cavity Using the Discrete Ordinates Method, *International Journal of Heat and Mass Transfer, 47* (2004), 2, pp. 257-269
[7] Mahapatra, S. K., *et al.*, Interaction of Surface Radiation and Variable Property Natural-Convection in a Differentially Heated Square Cavity – A Finite Element Analysis, *International Journal of Numerical Methods for Heat and Fluid-flow, 9* (1999), 4, pp. 423-443
[8] Mezrhab, A., *et al.*, Computation of Combined Natural-Convection and Radiation Heat Transfer in a Cavity Having a Square Body at Its Center, *Applied Energy, 83* (2006), 9, pp. 1004-1023
[9] Mikhailenko, S. A., *et al.*, Natural-Convection Combined with Surface Radiation in a Rotating Cavity with an Element of Variable Volumetric Heat Generation, *Energy, 210* (2021), 118543
[10] Sun, H., *et al.*, Effect of Surface Radiation on the Breakdown of Steady Natural-Convection Flows in a Square, Air-Filled Cavity Containing a Centered Inner Body, *Applied Thermal Engineering, 31* (2011), 6, pp. 1252-1262
[11] El Moutaouakil, L., *et al.*, Natural-Convection and Surface Radiation Heat Transfer in a Square Cavity with an Inner Wavy body, *International Journal of Thermophysics*, *41* (2020), 109, pp. 1-21
[12] El Moutaouakil, L., *et al.*, Natural-Convection and Radiation in a Cavity with a Partially Heated Cylinder, *Journal of Thermophysics and Heat Transfer*, *35* (2021), 2, pp. 312-322
[13] Nia, M. F., *et al.*, Transient Combined Natural-Convection and Radiation in a Double Space Cavity with Conducting Walls, *International Journal of Thermal Sciences, 128* (2018), June, pp. 94-104
[14] Yang, G., Wu J., Effects of Natural-Convection, Wall Thermal Conduction, and Thermal Radiation on Heat Transfer Uniformity at a Heated Plate Located at the Bottom of a 3-D Rectangular Enclosure, *Numerical Heat Transfer, Part A, 69* (2016), 6, pp. 589-606
[15] Ghernoug, C., *et al.*, The Natural-Convection in Annular Space Located between Two Horizontal Eccentric Cylinders: The Grashof Number Effect, *Energy Procedia, 36* (2013), Dec., pp. 293-302
[16] Wu, S. Y., *et al.*, Effect of Aperture Position and Size on Natural-Convection Heat Loss of a Solar Heat-Pipe Receiver, *Applied Thermal Engineering, 31* (2011), 14, pp. 2787-2796
[17] Zhang, K., *et al.*, Two- and 3-D Numerical Simulations of Natural-Convection in a Cylindrical Envelope with an Internal Concentric Cylinder with Slots, *International Journal of Heat and Mass Transfer, 70* (2014), Mar., pp. 434-438
[18] Wu, S. Y., *et al.*, Numerical Investigation on Combined Natural-Convection and Radiation Heat Losses in one Side Open Cylindrical Cavity with Constant Heat Flux, *International Journal of Heat and Mass Transfer, 71* (2014), Apr., pp. 573-584
[19] Shen, Z. G., *et al.*, Experimental and Numerical Investigations of Combined Free Convection and Radiation Heat Transfer in an Upward-Facing Cylindrical Cavity, *International Journal of Thermal Sciences, 89* (2015), Mar., Mar., pp. 314-326
[20] Roy, N., *et al.*, Electrohydrodynamics and Thermal Radiation Effects on Natural-Convection Flow in an Enclosed Domain, *International Communications in Heat and Mass Transfer, 126* (2021), 105437
[21] Sieres, J., *et al.*, Natural-Convection Air-Flow in Vertical Upright-Angled Triangular Cavities under Realistic Thermal Boundary Conditions, *Thermal Science*, *20* (2016), 5, pp. 1407-1420
[22] Yang, G., *et al.* Flow Reversal and Entropy Generation Due to Buoyancy Assisted Mixed Convection in the Entrance Region of a 3-D Vertical Rectangular Duct, *International Journal of Heat and Mass Transfer*, *67* (2013), Dec., pp. 741-751
[23] Siegel, R., Howell, J., *Thermal Radiation Heat Transfer*, Taylor and Francis, New York, USA, 2002
[24] ***, OpenFOAM, User guide 2020, http://www.openfoam.com/documentation/user-guide, 2020
[25] Saravanan, S., Sivaraj, C., Coupled Thermal Radiation and Natural-Convection Heat Transfer in a Cavity with a Heated Plate Inside, *International Journal of Heat and Fluid-flow, 40* (2013), Apr., pp. 54-64

Paper submitted: May 23, 2022
Paper revised: August 9, 2022
Paper accepted: August 16, 2022